In situ electronic redistribution of NiCoZnP/NF heterostructure via Fe doping for boosting hydrazine oxidation and hydrogen evolution

Tongtong Shi [b], Bo Gao [b], Haoyu Meng [b], Yumo Fu [b], Delong Kong [d], Penghui Ren [e], Haiyang Fu[b] and Zhongbao Feng [a,b,c*]

[a]*Key Laboratory for Ecological Metallurgy of Multimetallic Mineral (Ministry of Education), Northeastern University, Shenyang, 110819, China*

[b]*School of Metallurgy, Northeastern University, Shenyang, Liaoning 110819, China*

[c]*Engineering Research Center of Frontier Technologies for Low-carbon Steelmaking (Ministry of Education), Liaoning Low-carbon Steelmaking Technology Engineering Research Center, Shenyang 110819, China*

[d]*College of Chemistry, Chemical Engineering and Materials Science, Zaozhuang University, Zaozhuang 277160, China*

[e]*Shandong Laboratory of Advanced Materials and Green Manufacturing at Yantai, Yantai 264000, China*

[*] Corresponding author. E-mail address: fengzb@smm.neu.edu.cn (Z. Feng)

Experimental section

Chemicals

The following chemicals were used without further treatment: zinc nitrate hexahydrate ($Zn(NO_3)_2 \cdot 6H_2O$), nickel nitrate hexahydrate ($Ni(NO_3)_2 \cdot 6H_2O$), ferric nitrate nonahydrate ($Fe(NO_3)_3 \cdot 9H_2O$), cobalt nitrate hexahydrate ($Co(NO_3)_2 \cdot 6H_2O$), urea (H_2NCONH_2), sodium hypophosphite monohydrate ($NaH_2PO_2 \cdot H_2O$), hydrazine hydrate ($N_2H_4 \cdot H_2O$), and potassium hydroxide (KOH) were purchased from Aladdin Reagents Ltd. Commercial Pt/C (carbon containing 20 wt% Pt) and nickel foam (NF) were provided by Hesen Corporation and Shenzhen Kejingxing Technology Company, respectively.

Characterizations

The phase of the electrocatalysts was examined by X-ray diffraction (XRD, Rigaku Smartlab diffractometer). The morphology of the electrocatalysts was recorded by transmission electron microscopy (TEM, JEM-2100F) and scanning electron microscope (SEM, SU8010, Hitachi). X-ray photoelectron spectroscopy (XPS, VG Scientific ESCALab250i-XL) was carried out to measure valence states of the catalysts.

Electrochemical measurements

Electrochemical HER and HzOR performance were measured employing CHI760e workstation in a three-electrode cell with 1 M KOH and 1 M KOH with 0.5 M $N_2H_4 \cdot H_2O$ electrolyte, respectively. The catalysts/NF was served as working electrode, and Pt sheet and SCE were used as counter electrode and reference electrode, respectively. The HER and HzOR activities were measured by linear sweep voltammetry (LSV) with *IR* compensation at 5 $mV \cdot s^{-1}$. All potentials were related to reversible hydrogen electrode (RHE): $E_{RHE} = E_{SCE} + 0.059pH + 0.241$ without special illustration. Electrochemical surface area (ECSA) was measured by cyclic voltammetry (CV) with different scan rates to determine the double-layer capacitance (C_{dl}). Electrochemical impedance spectroscopy (EIS) was performed from 10^5 to10^{-2} Hz. The stability of the samples was determined by chronoamperometry and multi-current plot. The overall hydrazine splitting (OHzS) and overall water splitting (OWS) were performed in a double-electrode electrolyzer by employing Fe-NiCoZnP/NF as both cathodic and anodic electrodes in 1 M KOH with 0.5 M $N_2H_4 \cdot H_2O$ and 1 M KOH, respectively.

DFT Calculations

Theoretically calculations were performed with Vienna Ab Initio Simulation Package (VASP) according to density functional theory (DFT). Electronic exchange-correction interaction was determined by GGA with Predew-Burke and Ernzerhof (PBE). The energy cutoff of 450 eV and iteration of 10^{-5} eV were adopted. A 15 Å vacuum was employed to separate the slab in z direction. A k-point mesh (3∗3∗1) was applied. The Gibbs free energy (ΔG) for the intermediates was calculated by $\Delta G = \Delta E + \Delta ZPE - T\Delta S$, where ΔE, ΔZPE and ΔS are the adsorption energy change, zero-point energy change and entropy change, respectively.

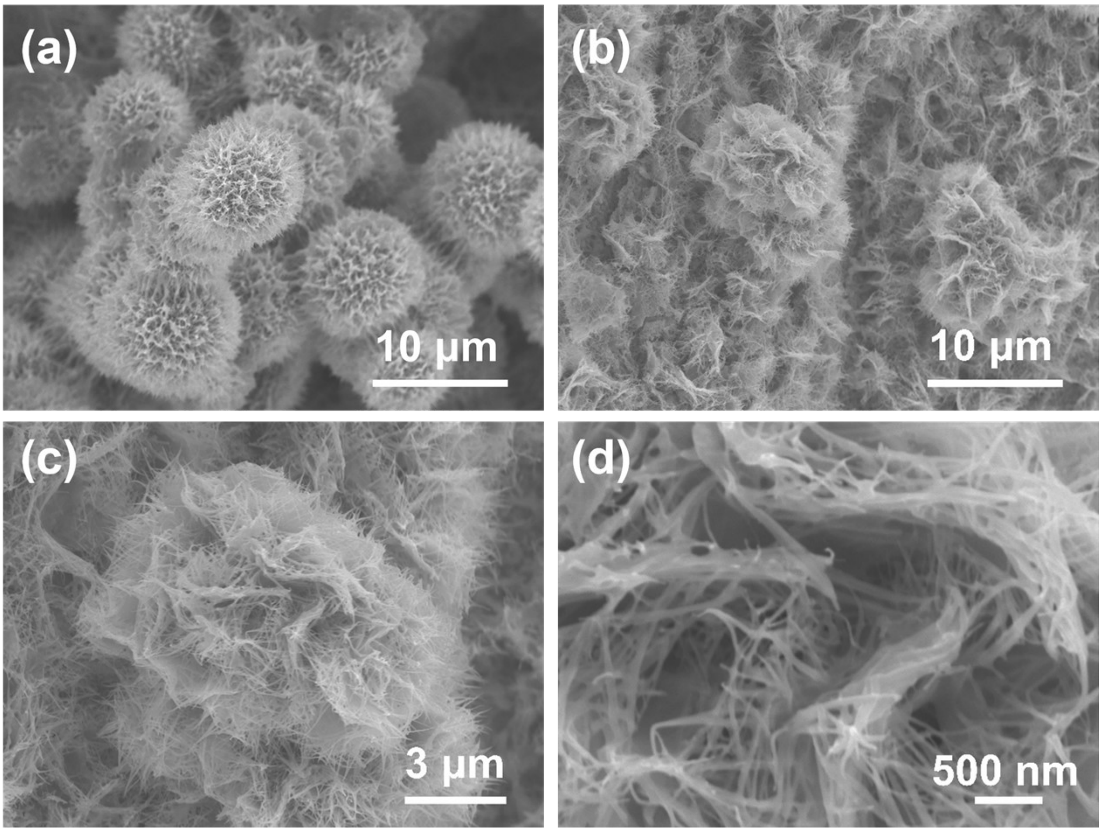

Fig. S1 SEM images of (a) Fe-NiCoZnP/NF and (b-d) NiCoZnP/NF.

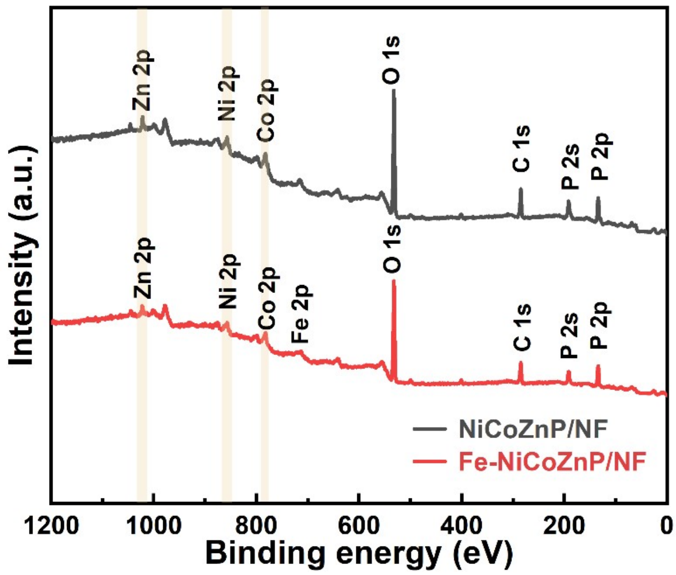

Fig. S2 XPS survey spectra of NiCoZnP/NF and Fe-NiCoZnP/NF.

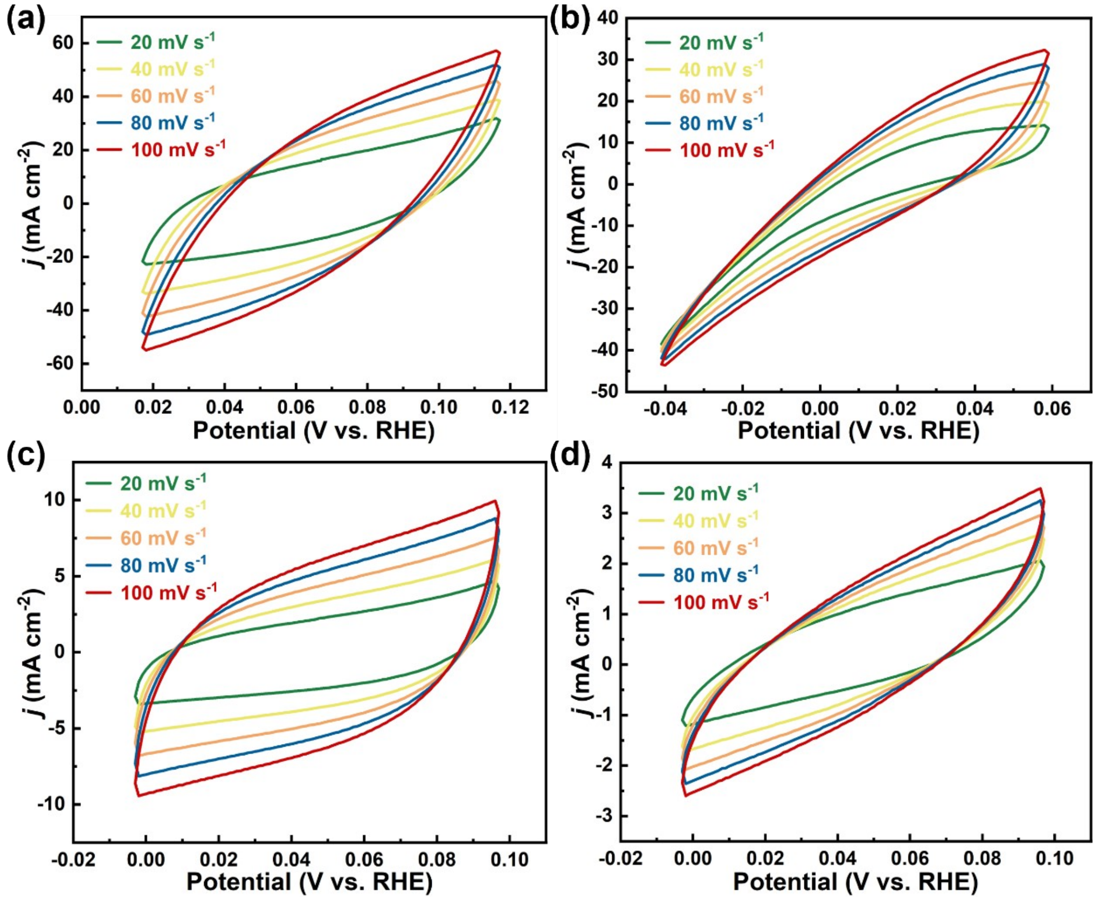

Fig. S3 HER CV plots of (a) Fe-NiCoZnP/NF; (b) NiCoZnP/NF; (c) Pt/C and (d) NF at various scan rates in 1 M KOH electrolyte.

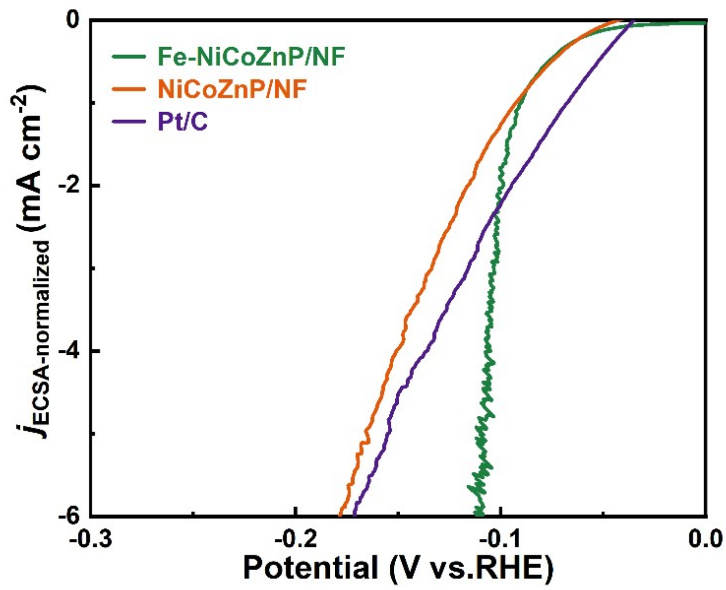

Fig. S4 HER LSV plots of Fe-NiCoZnP/NF, NiCoZnP/NF and Pt/C after averaged by ECSA.

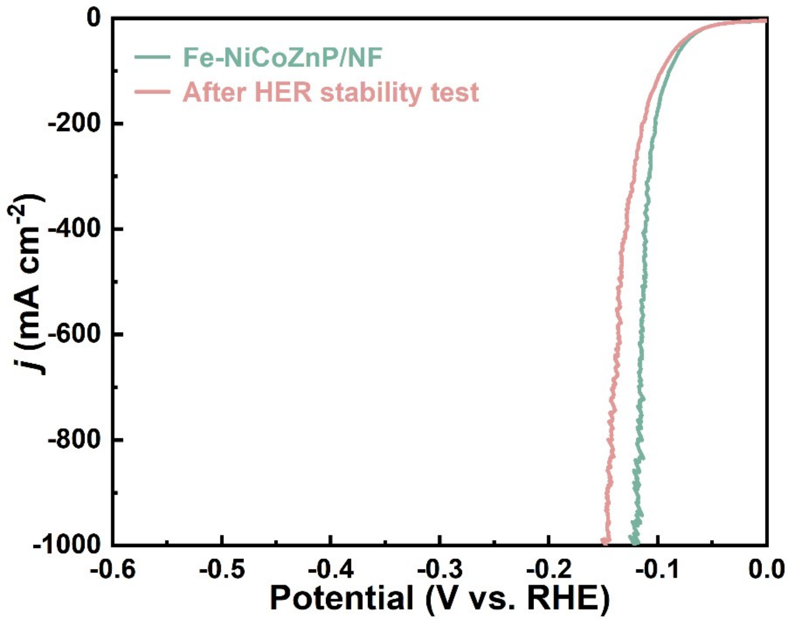

Fig. S5 LSV plots of Fe-NiCoZnP/NF before and after HER stability tests.

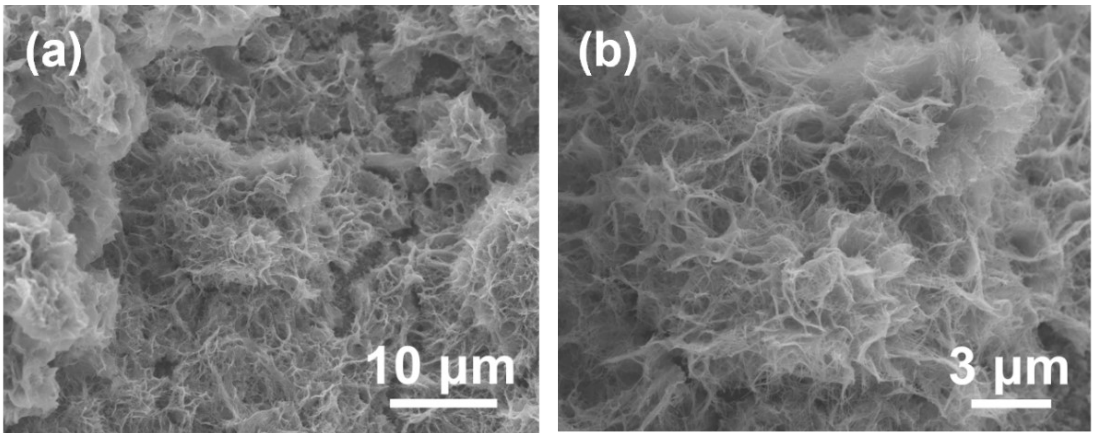

Fig. S6 SEM images of Fe-NiCoZnP/NF after HER stability test.

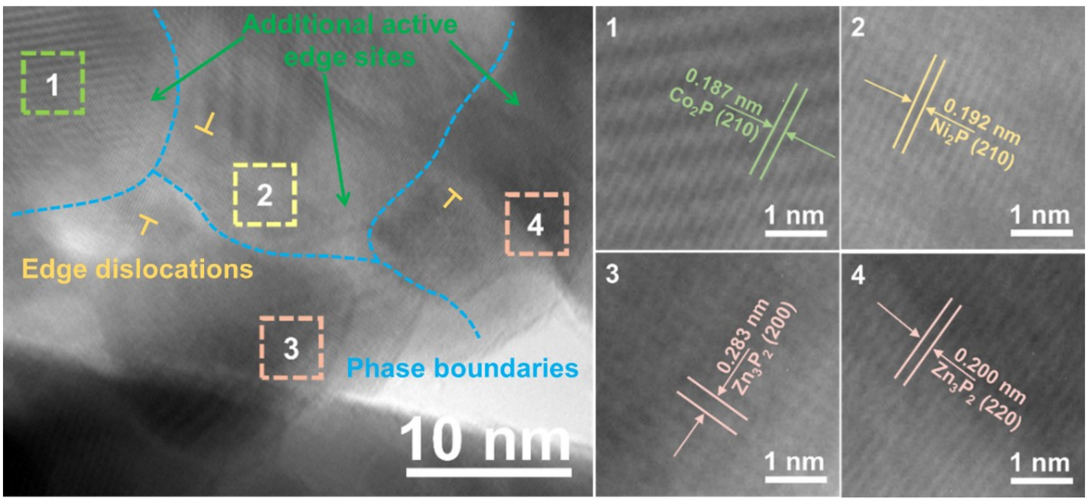

Fig. S7 TEM images of Fe-NiCoZnP/NF after HER stability test.

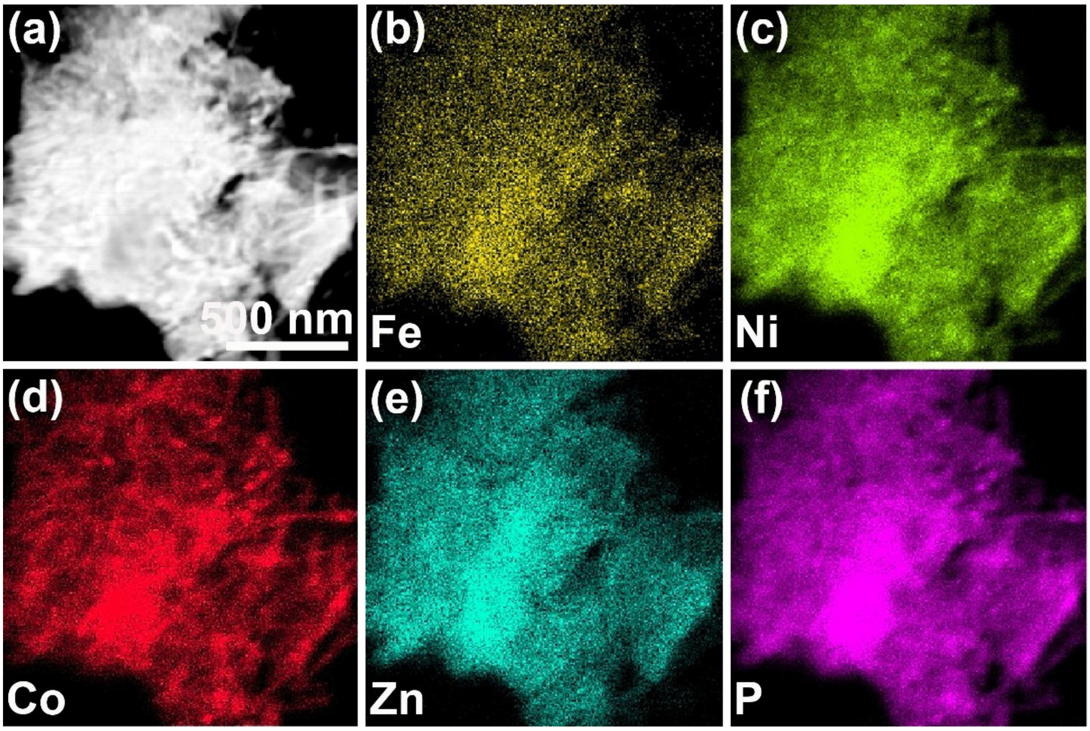

Fig. S8 (a) HADDF-STEM image and (b-f) TEM-EDS mapping images of Fe, Ni, Co, Zn and P of Fe-NiCoZnP/NF after HER stability test.

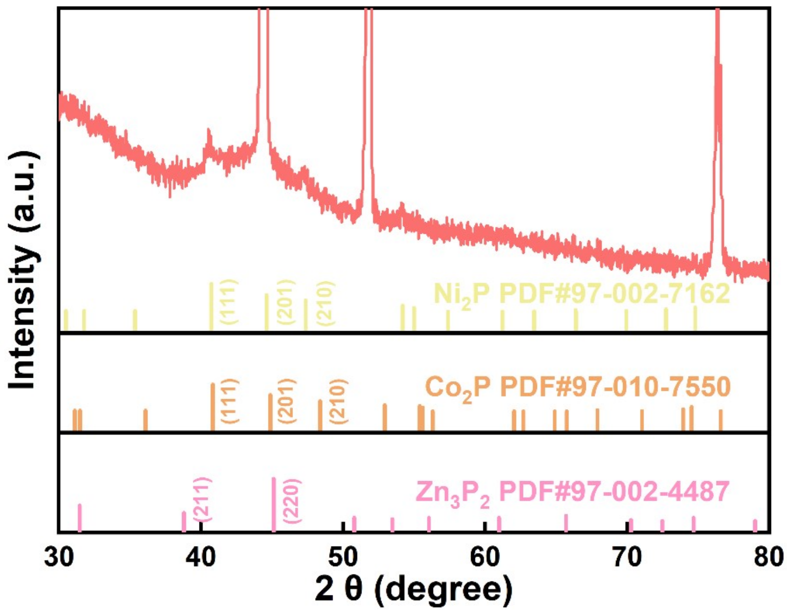

Fig. S9 XRD pattern of Fe-NiCoZnP/NF after HER stability test.

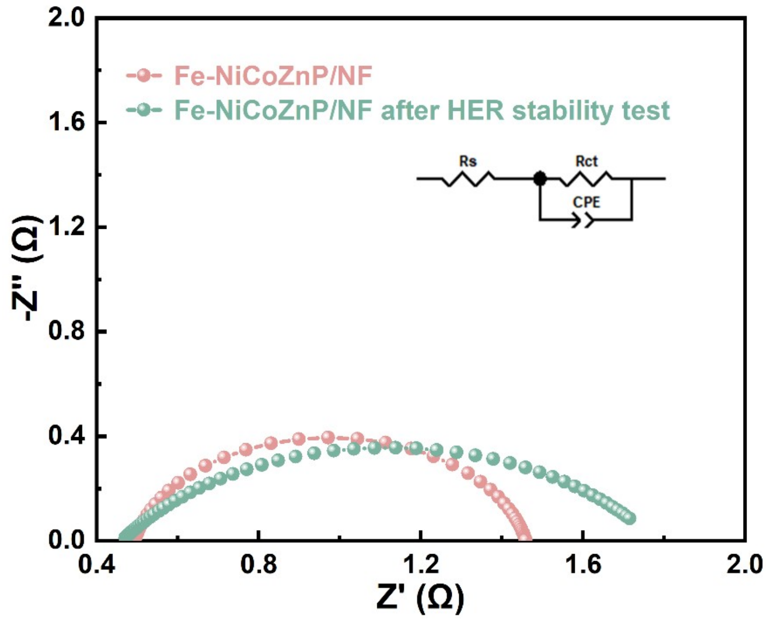

Fig. S10 EIS results of Fe-NiCoZnP/NF before and after HER stability tests and the inset equivalent circuit model.

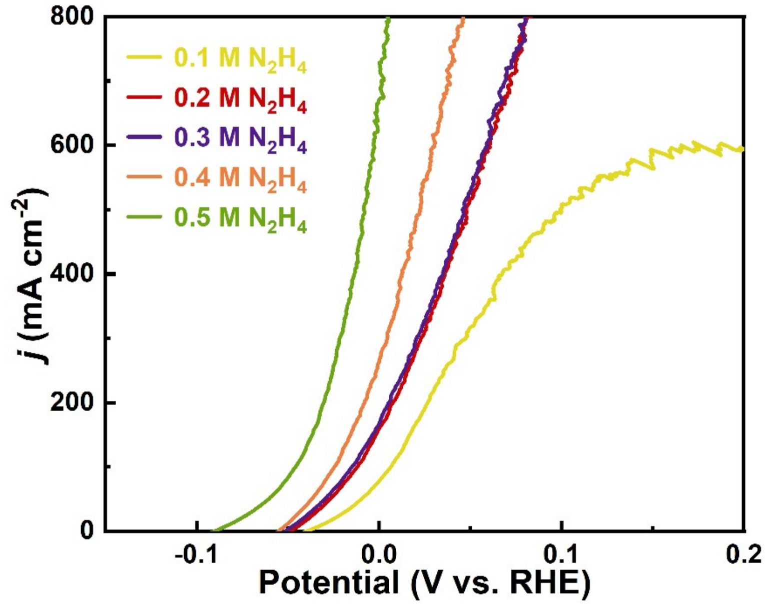

Fig. S11 LSV curves of Fe-NiCoZnP/NF in 1.0 M KOH with various N_2H_4 H_2O concentration.

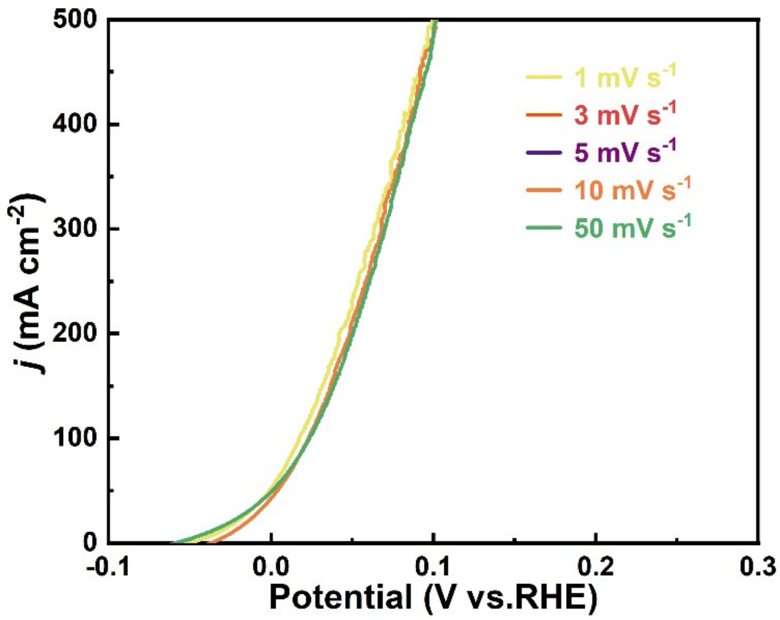

Fig. S12 LSV curves of Fe-NiCoZnP/NF at different scan rates in 1 M KOH with 0.5 M N_2H_4 H_2O electrolyte.

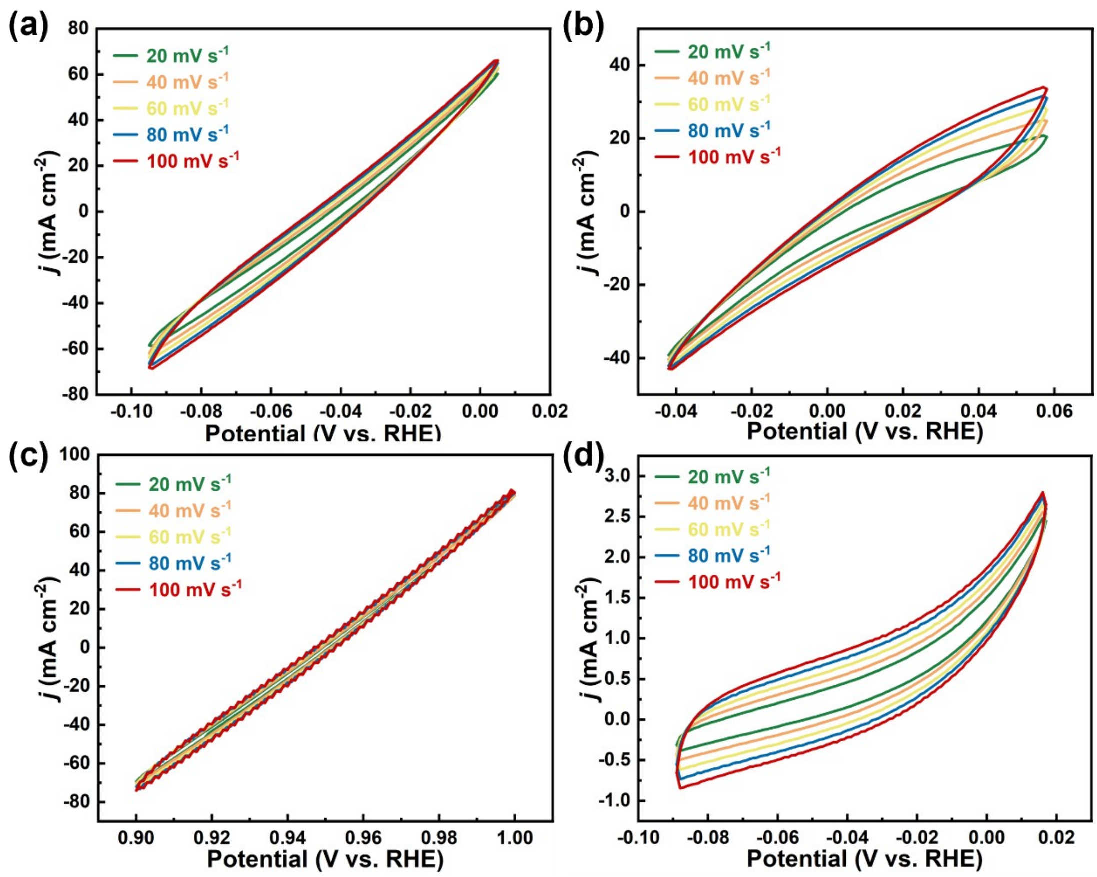

Fig. S13 HzOR CV plots of (a) Fe-NiCoZnP/NF; (b) NiCoZnP/NF; (c) Pt/C and (d) NF at various scan rates in 1 M KOH with 0.5 M N_2H_4 H_2O electrolyte.

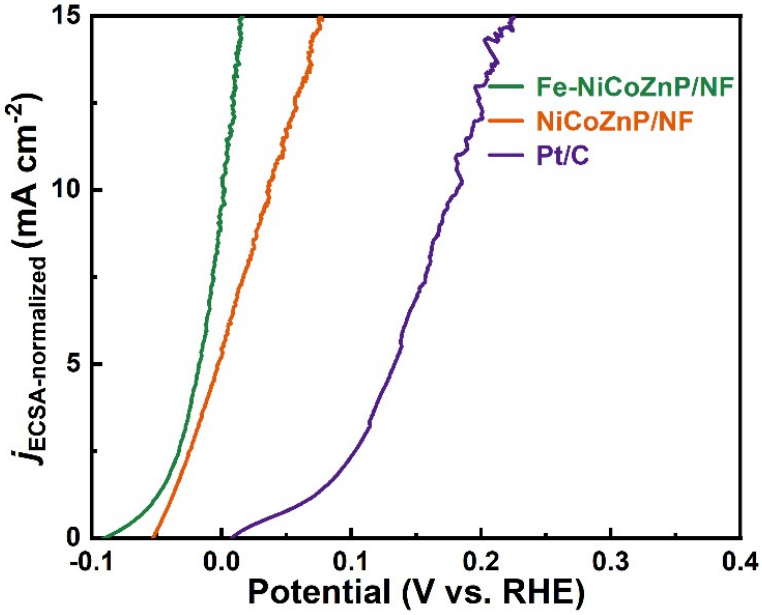

Fig. S14 HzOR LSV curves of Fe-NiCoZnP/NF, NiCoZnP/NF and Pt/C after averaged by ECSA.

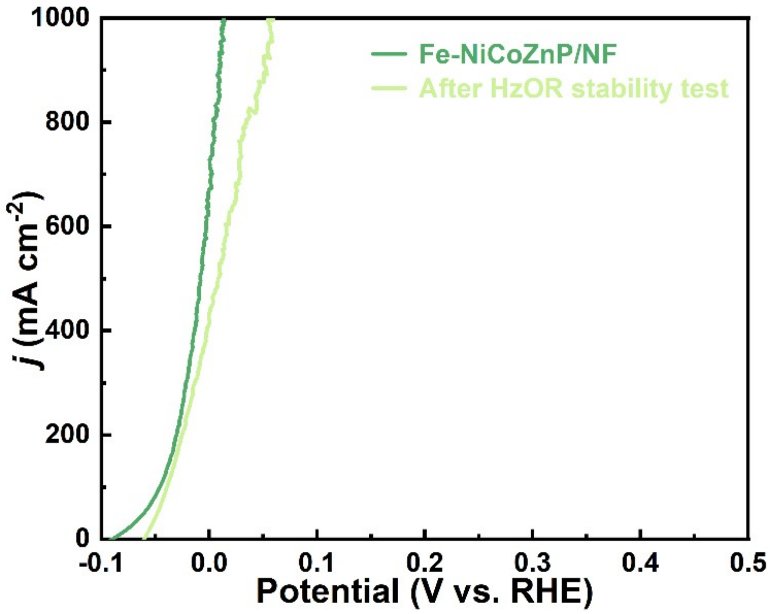

Fig. S15 HzOR LSV curves of Fe-NiCoZnP/NF before and after HzOR stability tests.

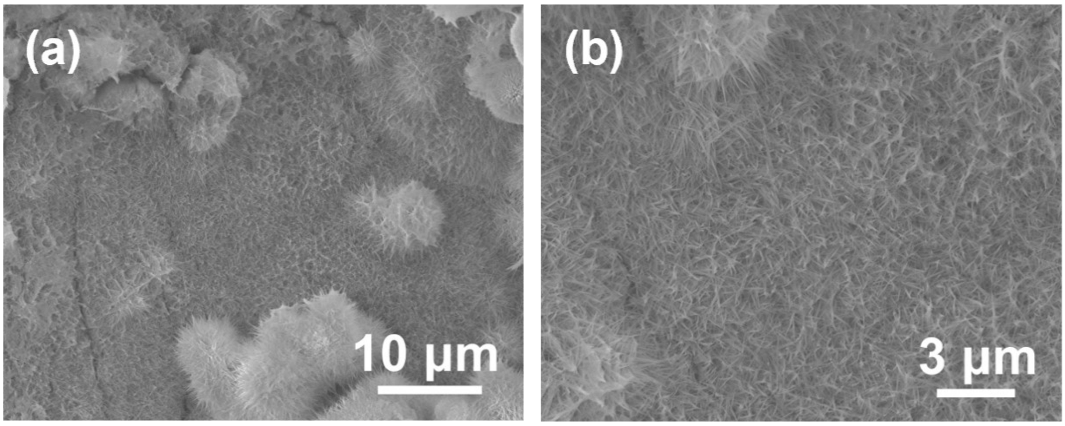

Fig. S16 SEM images of Fe-NiCoZnP/NF after HzOR stability test.

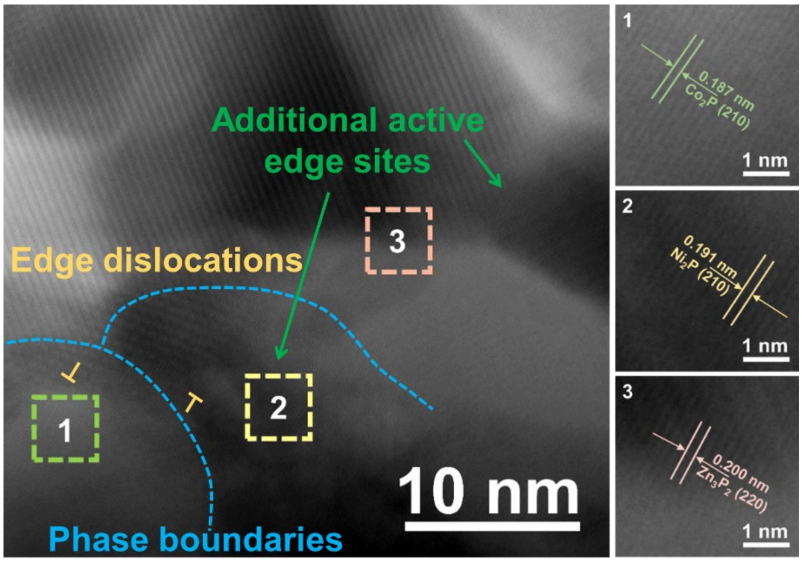

Fig. S17 TEM images of Fe-NiCoZnP/NF after HzOR stability test.

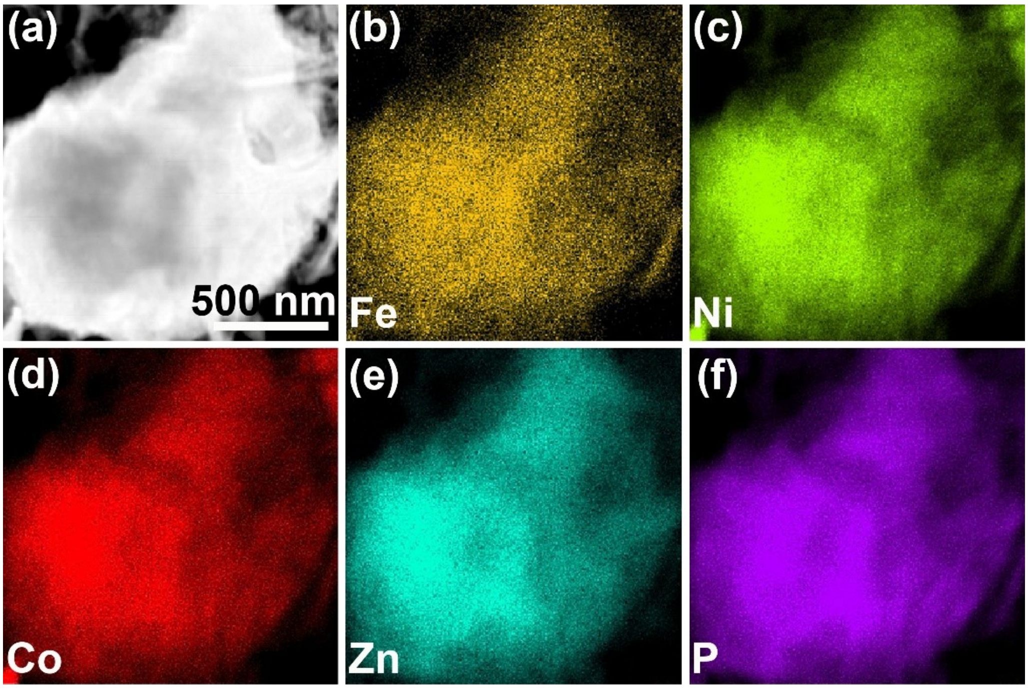

Fig. S18 (a) HADDF-STEM image and (b-f) TEM-EDS mapping images of Fe, Ni, Co, Zn and P of Fe-NiCoZnP/NF after HzOR stability test.

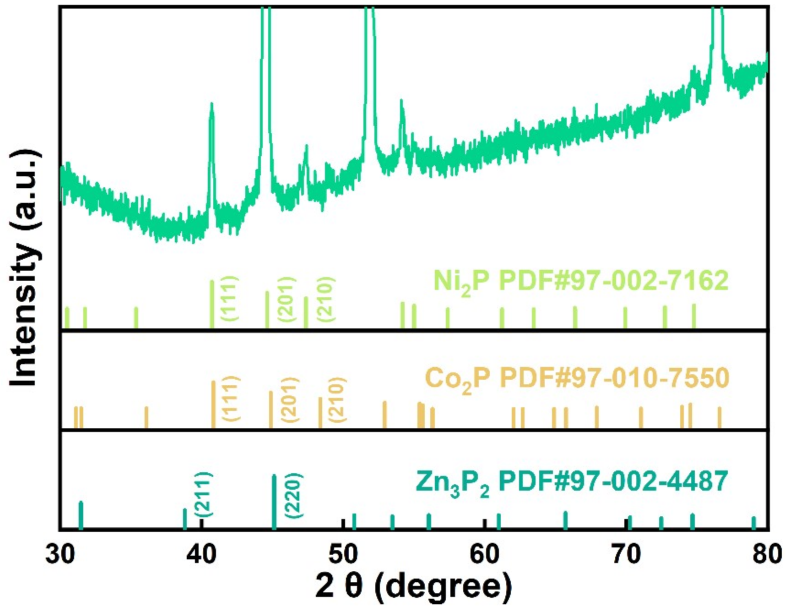

Fig. S19 XRD pattern of Fe-NiCoZnP/NF after HzOR stability test.

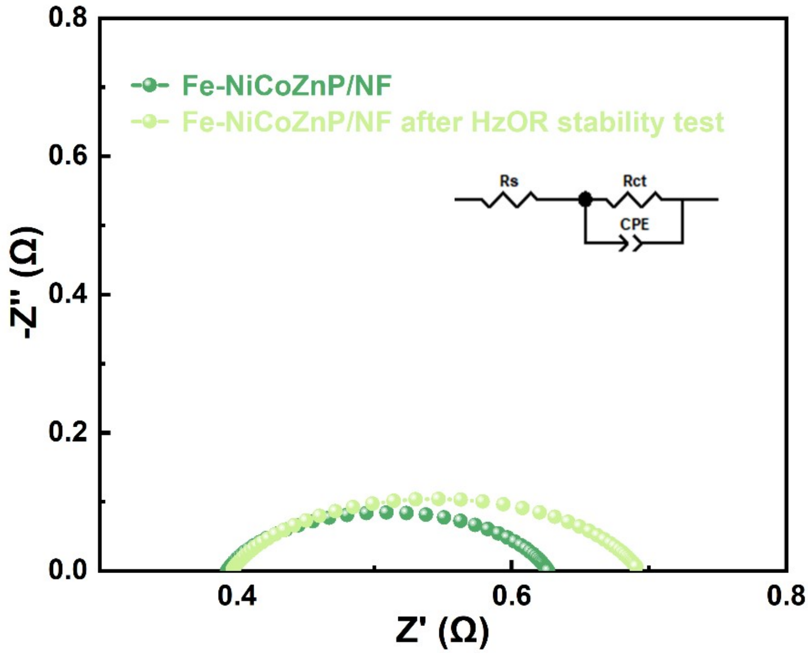

Fig. S20 EIS results of Fe-NiCoZnP/NF before and after HzOR stability tests.

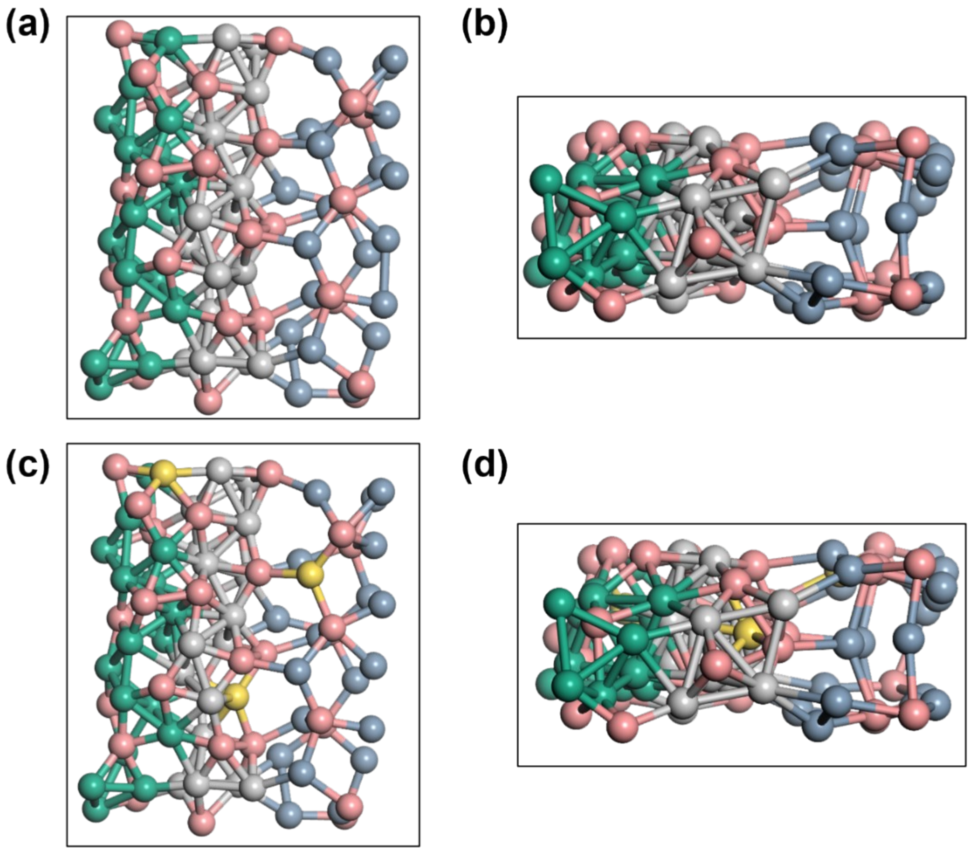

Fig. S21 Top (upper) and side (lower) views of the optimized structures of (a-b) NiCoZnP/NF and (c-d) Fe-NiCoZnP/NF.

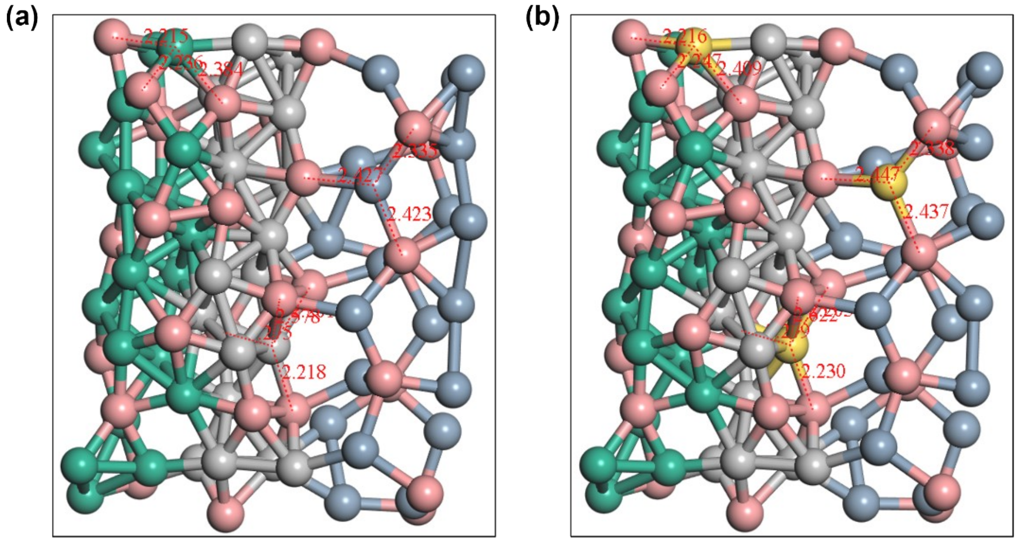

Fig. S22 (a) NiCoZnP/NF and (b) Fe-NiCoZnP/NF models with serial numbers.

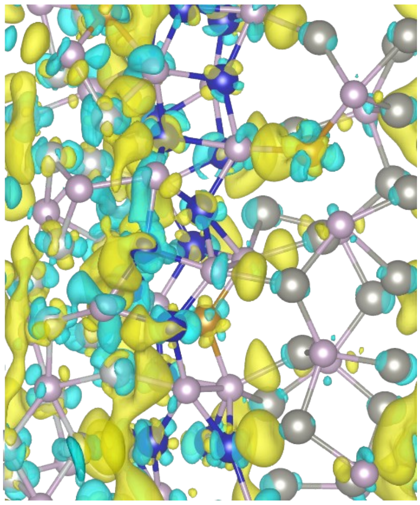

Fig. S23 Charge density distribution for the interface of Fe-NiCoZnP/NF**.**

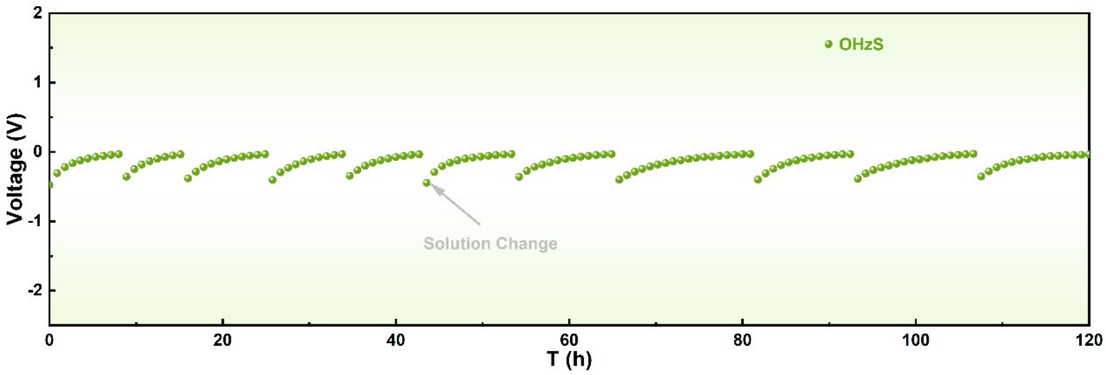

Fig. S24 Chronopotentiometic plots of Fe-NiCoZnP/NF || Fe-NiCoZnP/NF couple for 120 h at 100 mA cm^{-2}.

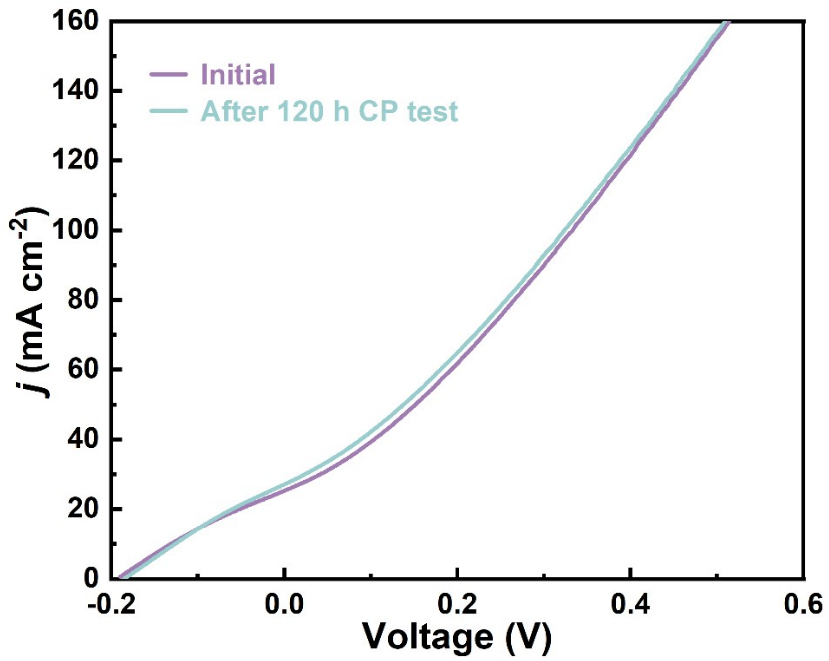

Fig. S25 LSV curves of Fe-NiCoZnP/NF ǁ Fe-NiCoZnP/NF couple before and after chronopotentiometry (CP) tests.

Table S1 A survey of the catalytic performance of various electrocatalysts for HER.

Electrocatalysts	Electrolyte	Electrocatalytic performance		Ref.
	KOH (mol·L^{-1})	j (mA·cm^{-2})	Overpotential (mV)	
Ni-Co-P/NF	1.0	10	37	[S1]
		100	115	
		1000	280	
Fe-Ni_2P_v	1.0	100	87	[S2]
		1000	~200	
FeNiP-NPHC	1.0	10	65	[S3]
		100	182	
N-Ni_5P_4@CoP/CFP	1.0	10	56	[S4]
$(Fe_{1-x}Co_x)_2P/Ni_3N$	1.0	100	113	[S5]
PW-Co_3N/NF	1.0	10	41	[S6]
		100	130	
Ni_2P/Zn-Ni-P	1.0	10	63	[S7]
NiP_2-650(*c/m*)	1.0	10	63	[S8]
FeNiP@p-NPCF/CC	1.0	10	89	[S9]
V-$Ni_2P/Ni_{12}P_5$	1.0	10	62	[S10]
Ru SAs-Ni_2P	1.0	10	57	[S11]
$NiP_2/NiSe_2$	1.0	10	93	[S12]
		100	160	
$Ni_5P_{4-x}I_x/Ni_2P$	1.0	10	45	[S13]

Fe (pFe/FeP)	1.0	100	380	[S14]
O-NiMoP/NF	1.0	10	54	[S15]
		10	**35**	
Fe-NiCoZnP/NF	**1.0**	**100**	**89**	**This work**
		1000	**121**	

Table S2 A survey of the catalytic performance of various electrocatalysts for HzOR

Electrocatalysts	**Electrolyte**	**Electrocatalytic performance**		**Ref.**
	N_2H_4/KOH ($mol \cdot L^{-1}$)	***j*** **($mA \cdot cm^{-2}$)**	**Potential (mV vs. RHE)**	
$N-Ni_5P_4$@CoP/CFP	0.1,1.0	10	-32	[S4]
		100	60	
$Cu_1Co_2-Ni_2P$/NF	0.1, 1.0	10	-52	[S16]
$NiMo/Ni_2P$/NF	0.5, 1.0	10	-17	[S17]
		100	32	
Ru_1-NiCoP	0.3, 1.0	10	-60	[S18]
Ru/PNC	0.5, 1.0	10	-20.4	[S19]
Ni-C HNSA	0.1, 1.0	10	-20	[S20]
$Ni(OH)_2/Ni_2P$/NF	0.5, 1.0	10	-14	[S21]
		100	73.9	
$RuFe-Ni_2P$@NF	0.5, 1.0	100	~40	[S22]
		1000	~230	
$P/Fe-NiSe_2$	0.7, 1.0	100	200	[S23]
FHNNP/NF	0.4, 1.0	10	-44	[S24]

		100	0.1	
NiCo-$MoNi_4$	0.1, 1.0	10	-30	[S25]
Ru-FeP_4/IF	0.5, 1.0	1000	335	[S26]
CoFeNiCrMnP/NF	0.4, 1.0	10	-79	[S27]
		100	-62	
CoH-CoP_v@CFP	0.5, 1.0	10	-60	[S28]
Ni NCNA	0.3, 1.0	10	-26	[S29]
Fe-NiCoZnP/NF	**0.5, 1.0**	**10**	**-82**	**This work**
		100	**-46**	
		1000	**15**	

Table S3 The cell voltage comparisons of OHzS.

Electrocatalysts	Electrolyte N_2H_4/KOH (mol·L^{-1})	Electrocatalytic performance j (mA·cm^{-2})	Cell voltage (V)	Ref.
FeNiP-NPHC	0.5, 1.0	10	0.05	[S3]
Ni_2P/Zn-Ni-P	0.1, 1.0	10	0.165	[S7]
		100	0.558	
FeNiP@p-NPCF/CC	0.5, 1.0	10	0.05	[S9]
Cu_1Co_2-Ni_2P/NF	0.1, 1.0	10	0.16	[S16]
		100	0.39	
P/Fe-$NiSe_2$	0.7, 1.0	10	0.09	[S23]
		100	0.445	
Ni_3N-Co_3NPNAs/NF	0.1, 1.0	10	~0.15	[S30]
		100	0.668	

NiCo@C/MXene	0.5, 1.0	10 100	~0.05 ~0.36	[S31]
Ru_2P/C-PAN	0.3, 1.0	10 100	0.03 0.35	[S32]
Ni(Cu)@NiFeP/NM	0.5,1.0	10 100	0.147 0.491	[S33]
CoP/NCNT-CP	0.5, 1.0	10	0.89	[S34]
Fe-NiCoZnP/NF	**0.5, 1.0**	**10** **100**	**0.03** **0.33**	**This work**

References

[S1] L. Zhu, J. Huang, G. Meng, T. Wu, C. Chen, H. Tian, Y. Chen, F. Kong, Z. Chang, X. Cui and J. Shi, Active site recovery and N-N bond breakage during hydrazine oxidation boosting the electrochemical hydrogen production, Nat. Commun., 2023, **14**, 1997.

[S2] X. Liu, Q. Yu, X. Qu, X. Wang, J. Chi and L. Wang, Manipulating electron redistribution in Ni_2P for enhanced alkaline seawater electrolysis, Adv. Mater., 2023, 2307395.

[S3] Q. Yu, X. Liu, G. Liu, X. Wang, Z. Li, B. Li, Z. Wu and L. Wang, Constructing three-phase heterojunction with 1D/3D hierarchical structure as efficient trifunctional electrocatalyst in alkaline seawater, Adv. Funct. Mater., 2022, **32**, 2205767.

[S4] S. Zhang, C. Zhang, X. Zheng, G. Su, H. Wang and M. Huang, Integrating electrophilic and nucleophilic dual sites on heterogeneous bimetallic phosphide via enhancing interfacial electronic field to boost hydrazine oxidation and hydrogen evolution, Appl. Catal. B: Environ., 2023, **324**, 122207.

[S5] W. Ma, D. Li, L. Liao, H. Zhou, F. Zhang, X. Zhou, Y. Mo and F. Yu, High-performance bifunctional porous iron-rich phosphide/nickel nitride heterostructures for alkaline seawater splitting, Small, 2023, **19**, 2207082.

[S6] Y. Liu, J. Zhang, Y. Li, Q. Qian, Z. Li, Y. Zhu and G. Zhang, Manipulating dehydrogenation kinetics through dual-doping Co_3N electrode enables highly efficient hydrazine oxidation assisting self-powered H_2 production, Nat. Commun., 2020, **11**, 1853.

[S7] Y. Li, X. Yu, J. Gao and Y. Ma, Hierarchical Ni_2P/Zn-Ni-P nanosheet array for efficient energy-saving hydrogen evolution and hydrazine oxidation, J. Mater. Chem. A, 2023, **11**, 2191-2202.

[S8] Q. Fu, X. Wang, J. Han, J. Zhong, T. Zhang, T. Yao, C. Xu, T. Gao, S. Xi, C. Liang, L. Xu, P. Xu and B. Song, Phase-junction electrocatalysts towards enhanced hydrogen evolution reaction in alkaline media, Angew. Chem. Int. Ed., 2021, **133**, 263-271.

[S9] J.T. Ren, L. Chen, L. Wang, X.L. Song, Q.H. Kong and Z.Y. Yuan, Multifunctional metal-phosphide-based electrocatalysts for highly efficient solar hydrogen production integrated devices, J. Mater. Chem. A, 2023, **11**, 2899-2909.

[S10] T. Zhao, S. Wang, Y. Li, C. Jia, Z. Su, D. Hao, B. Ni, Q. Zhang and C. Zhao, Heterostructured V-doped $Ni_2P/Ni_{12}P_5$ electrocatalysts for hydrogen evolution in anion exchange membrane water electrolyzers, Small, 2022, **18**, 2204758.

[S11] K. Wu, K. Sun, S. Liu, W.C. Cheong, Z. Chen, C. Zhang, Y. Pan, Y. Cheng, Z. Zhuang, X. Wei, Y. Wang, L. Zheng, Q. Zhang, D. Wang, Q. Peng, C. Chen and Y. Li, Atomically dispersed Ni-Ru-P interface sites for high-efficiency pH-universal electrocatalysis of hydrogen evolution, Nano Energy, 2021, **80**, 105467.

[S12] L. Yang, L. Huang, Y. Yao and L. Jiao, In-situ construction of lattice-matching $NiP_2/NiSe_2$ heterointerfaces with electron redistribution for boosting overall water splitting, Appl. Catal. B: Environ., 2021, **282**, 119584.

[S13] T. Xu, D. Jiao, M. Liu, L. Zhang, X. Fan, L. Zheng, W. Zheng and X. Cui, Ni center coordination reconstructed nanocorals for efficient water splitting, Adv. Sci., 2021, **10**, 2205605.

[S14] C. Xiao, R.R. Gaddam, Y. Wu, X. Sun, Y. Liang, Y. Li and X.S. Zhao, Improvement of the electrocatalytic performance of FeP in neutral electrolytes with Fe nanoparticles, Chem. Eng. J., 2021, **408**, 127330.

[S15] H. Jiang, M. Sun, S. Wu, B. Huang, C.S. Lee and W. Zhang, Oxygen-incorporated NiMoP nanotube arrays as efficient bifunctional electrocatalysts for urea-assisted energy-saving hydrogen production in alkaline electrolyte, Adv. Funct. Mater., 2021, **31**, 2104951.

[S16] C. Feng, M. Lv, J. Shao, H. Wu, W. Zhou, S. Qi, C. Deng, X. Chai, H. Yang, Q. Hu and C. He, Lattice strain engineering of Ni_2P enables efficient catalytic hydrazine oxidation-assisted hydrogen production, Adv. Mater., 2023, **35**, 2305598.

[S17] Y. Yang, X. Li, G. Liu, H. Liu, Y. Shi, C. Ye, Z. Fang, M. Ye and J. Shen, Hierarchical ohmic contact interface engineering for efficient hydrazine-assisted hydrogen evolution reaction, Adv. Mater., 2023, 2307979.

[S18] Y. Hu, T. Chao, Y. Li, P. Liu, T. Zhao, G. Yu, C. Chen, X. Liang, H. Jin, S. Niu, W. Chen, D. Wang and Y. Li, Cooperative Ni(Co)-Ru-P sites activate dehydrogenation for hydrazine oxidation assisting self-powered H_2 production, Angew. Chem. Int. Ed., 2023, **135**, 202308800.

[S19] X. Guan, Q. Wu, H. Li, S. Zeng, Q. Yao, R. Li, H. Chen, Y. Zheng and K. Qu, Identifying the roles of Ru single atoms and nanoclusters for energy-efficient hydrogen production assisted by electrocatalytic hydrazine oxidation, Appl. Catal. B: Environ., 2021, **323**, 122145.

[S20] Y. Zhu, J. Zhang, Q. Qian, Y. Li, Z. Li, Y. Liu, C. Xiao, G. Zhang and Y. Xie, Dual nanoislands on Ni/C hybrid nanosheet activate superior hydrazine oxidation-assisted high-efficiency H_2 production, Angew. Chem. Int. Ed., 2022, **61**, 202113082.

[S21] H.M. Yang, H.Y. Wang, M.L. Sun and Z.Y. Yuan, Interface engineering of bifunctional nickel hydroxide/nickel phosphide heterostructure for efficient intermittent hydrazine-assisted water splitting, Chem. Eng. J., 2023, **475**, 146134.

[S22] X. Zhai, Q. Yu, J. Chi, X. Wang, B. Li, B. Yang, Z. Li, J. Lai and L. Wang, Accelerated dehydrogenation kinetics through Ru, Fe dual-doped Ni_2P as bifunctional electrocatalyst for hydrazine-assisted self-powered hydrogen generation, Nano Energy, 2023, **105**, 108008.

[S23] H.Y. Wang, L. Wang, J.T. Ren, W.W. Tian, M.L. Sun and Z.Y. Yuan, Heteroatom-Induced accelerated kinetics on nickel selenide for highly efficient hydrazine-assisted water splitting and Zn-hydrazine battery, Nano-Micro Lett., 2023, **15**, 155.

[S24] S. Zhang, X. Wei, S. Dai, H. Wang and M. Huang, Efficient hydrazine electro-oxidation achieved by tailored electron injection into Fe (III) sites activating dehydrogenation, Adv. Funct. Mater., 2023, 2311370.

[S25] Q. Qian, Y. Li, Y. Liu, Y. Guo, Z. Li, Y. Zhu and G. Zhang, Hierarchical multi-component nanosheet array electrode with abundant NiCo/$MoNi_4$ heterostructure interfaces enables superior bifunctionality towards hydrazine oxidation assisted energy-saving hydrogen generation, Chem. Eng. J., 2021, **414**, 128818.

[S26] T. Cui, J. Chi, J. Zhu, X. Sun, J. Lai, Z. Li and L. Wang, Tuning the size and chemisorption of FeP_4 by trace Ru doping for hydrazine-assisted hydrogen evolution in seawater at large-current-density, Appl. Catal. B: Environ., 2022, **319**, 121950.

[S27] K. Li, J. He, X. Guan, Y. Tong, Y. Ye, L. Chen and P. Chen, Phosphorus-modified amorphous high-entropy CoFeNiCrMn compound as high-performance electrocatalyst for hydrazine-assisted water electrolysis, Small, 2023, **19**, 2302130.

[S28] X. Wei, S. Zhang, X. Lv, S. Dai, H. Wang and N. Huang, Local-reconstruction enables cobalt phosphide array with bifunctional hydrogen evolution and hydrazine oxidation, Appl. Catal. B: Environ., 2023, 123661.

[S29] Y. Li, J. Li, Q. Qian, X. Jin, Y. Liu, Z. Li, Y. Zhu, Y. Guo, Y. Guo and G. Zhang, Superhydrophilic Ni-based multicomponent nanorod-confined-nanoflake array electrode achieves waste-battery-driven hydrogen evolution and hydrazine, Small, 2021, **17**, 2008148.

[S30] Q. Qian, J. Zhang, J. Li, Y. Li, X. Jin, Y. Zhu, Y. Liu, Z. Li, A. El-Harairy, C. Xiao, G. Zhang and Y. Xie, Artificial heterointerfaces achieve delicate reaction kinetics towards hydrogen evolution and hydrazine oxidation catalysis, Angew. Chem. Int. Ed., 2021, **133**, 6049-6058.

[S31] F. Sun, J. Qin, Z. Wang, M. Yu, X. Wu, X. Sun and J. Qiu, Energy-saving hydrogen production by chlorine-free hybrid seawater splitting coupling hydrazine degradation, Nat. Commun., 2021, **12**, 4182.

[S32] Q. Qian, W. Wang, G. Wang, X. He, Y. Feng, Z. Li, Y. Zhu, Y. Zhang and G. Zhang, Phase-selective synthesis of ruthenium phosphide in hybrid structure enables efficient hybrid water electrolysis under pH-universal conditions, Small, 2022, **18**, 2200242.

[S33] Q. Sun, M. Zhou, Y. Shen, L. Wang, Y. Ma, Y. Li, X. Bo, Z. Wang and C. Zhao, Hierarchical nanoporous Ni(Cu) alloy anchored on amorphous NiFeP as efficient bifunctional electrocatalysts for hydrogen evolution and hydrazine oxidation, J. Catal., 2019, **373**, 180-189.

[S34] L. Wang, J. Cao, X. Cheng, C. Lei, Q. Dai, B. Yang, Z. Li, M. Younis, L. Lei, Y. Hou and K. Ostrikov, ZIF-derived carbon nanoarchitecture as a bifunctional pH-universal electrocatalyst for energy-efficient hydrogen evolution, ACS Sustain. Chem. Eng. 2019, **7**, 10044-10051.